Available online at https://link.springer.com/journal/42241
http://www.jhydrodynamics.com
Journal of Hydrodynamics, 2019, 31(5): 976-985
https://doi.org/10.1007/s42241-018-0146-y

A new method of dynamic mesh used in continuous guide vane closure of a reversible pump-turbine in generating mode *

Xiu-li Mao[1], Yuan Zheng[2], Giorgio Pavesi[3], Zhan-shan Xie[2]
1.*College of Water Resources and Architectural Engineering, Northwest A&F University, Yangling 712100, China*
2. *College of Water Conservancy and Hydropower Engineering, Hohai University, Nanjing 210098, China*
3. *Department of Industrial Engineering, University of Padua, Padova, Italy*

(Received August 1, 2017, Revised December 21, 2017, Accepted February 19, 2018, Published online November 30, 2018)

Abstract: In this paper, a new method of dynamic mesh based on two functional controls is used in the continuous guide vane closure, and the three-dimensional numerical simulation is carried out to investigate the transient flow characteristics for a Francis-type reversible pump-turbine in the turbine mode in the load regulation scenario，with the detached eddy simulation (DES) turbulent model. The transient flow characteristics during the closure of the guide vanes are illustrated by analyzing the signals of the mass flow, the torque and the pressure fluctuations in the frequency and time-frequency domains. It is shown by the simulated results that a continuous assessment of the transient flow characteristics during the guide vane closure may be made by using the new method of the dynamic mesh. Furthermore, the flow field analysis involves both the onset and the development of the unsteady phenomena progressively based on an organized guide vane closure law. The flow pattern in the return channel maintains a relatively stable flow field before the last stage of the closure, as compared with the unstable flow field in other domains. To identify the unit variation under the fluid-dynamical conditions, the influence of the three-dimensional unsteady flow structures in the passage is analyzed and its evolution during this transient process is characterized by the fluid-dynamics and the spectral analysis.

Key words: Francis-type reversible turbine, dynamic mesh, guide vane closure, flow characteristics

Introduction

The renewable energy technologies see a rapid and sustainable development, especially the wind and solar energies[1-2]. However, the renewable energies are extremely varied, and most of them pose a challenge for the stability of the grid, as well as their safe supply. Therefore for the use of the renewable energy, a collaborator is often required when the production is either too high or too low. In many cases the most efficient collaborator is a pumped storage plant, which delivers its long term energy storage and can serve as a producer (turbine) or a consumer (pump) in peak power situations[3-4]. As the heart of the pumped storage plant, the pump-turbine units are responsible for increasing the stability of the electrical power grid due to their excellent operating flexibility[5-7].

A reversible pump turbine (RPT) in the pumped storage plant can deal with the problems related to the conversion and the input of the energy into the grid, by switching between the pump and turbine modes[8-9]. However, the pump turbines have to pass through transient cycles during the power grid stabilization[10], in changing conditions between the pump and turbine modes, starting up and stopping of the unit, the load rejection and so on. It is highly desirable to change the speed and the frequency of the pump turbine to compromise the off-design conditions, as is shown in the S characteristics, moreover, these transient cycles are often accompanied with unstable flow conditions and high amplitude pressure pulsations[11]. In addition, the pressure amplitudes primarily depend on the instantaneous guide vane movement and the runner speed[12-13].

It was shown by the pressure measurements in the turbine draft tubes that the high amplitude pressure oscillations and the repeated fatigue loading on the runner blades during the load variation and the

* Project supported by the National Natural Science Foundation of China (Grant No. 51909222).
Biography: Xiu-li Mao (1991-), Female, Ph. D., Lecturer,
E-mail: maoxl@nwafu.edu.cn
Corresponding author: Yuan Zheng,
E-mail: zhengyuan@hhu.edu.cn

start-stop cycles are among the most important factors that affect the operating lifespan of the turbine components[14-15]. It is necessary and important to study these kinds of transient processes for the safe and stable operation of the unit[16-17].

The numerical simulation is the main approach to study the transient processes. Along with the improved capability of computer and the development of fluid dynamics, the numerical approach can well simulate the actual flow field[18]. Additionally, the inner flow in the machine is difficult to be measured, especially, the transient processes on the site, which pose many limitations.

In order to continuously evaluate the transient flow characteristics during the guide vane closure, 3-D numerical simulations are carried out to determine the off-design conditions of a reversible turbine in this paper, with a new dynamic mesh technique.

1. The new method of dynamic mesh

As mentioned before, the numerical simulation is now the main approach to investigate the inner flow field of an RPT. However, the poor mesh quality in a large scale mesh movement is a significant problem, for the validity of the numerical simulation. In the present work, a new method of the dynamic mesh is applied in the process of the fast guide vanes closure of the RPT in the turbine mode.

The new method of the dynamic mesh is a wall sliding mesh technique to improve the mesh quality, including: one part for the body nodes and the other for the wall mesh nodes. To be more specific, the guide vanes rotate around their respective axes, and their relative azimuth positions are continuously and independently adjustable to consider the influence of the relative position on the turbine characteristics. To improve the mesh quality, a program is developed to control the wall mesh node movement by counter rotating, and then the nodes move along the vane profile to achieve the mesh orthogonality.

2. Case study

The new method of the dynamic mesh is applied for an RPT model, during the process of the fast guide vane closure in the turbine mode. The dimensions of the numerical model for the turbine are similar to those used in the experimental measurements[19-20].

The model consists of one runner with 7 3-D backward blades, 22 adjustable guide vanes coupled with 11 return channel vanes, one diversion pipe and one draft tube (Fig. 1). Table 1 gives the main geometrical data of the considered RPT, where D is the diameter, B is the width, n is the number of blades of the relative domains, and α is the angle. The main regions of this model are shown in Fig. 2.

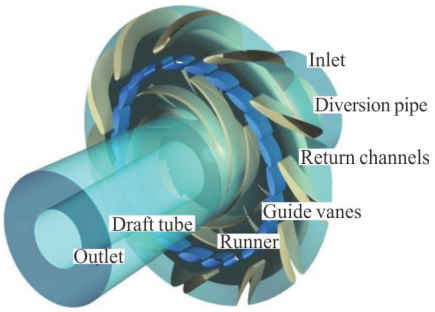

Fig. 1 (Color online) The main zones of the RPT model

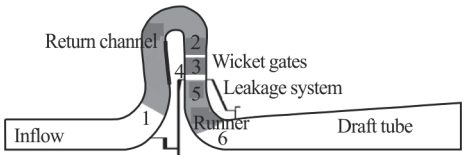

Fig. 2 Meridian view of RPT model with the regions filled in grey to refer to the blades and the regions filled in black to refer to the leakage system (1: Return channel inlet, 2: Return channel outlet, 3: Guide vane inlet, 4: Guide vane outlet, 5: Runner inlet, 6: Runner outlet)

Table 1 Main parameters of the RPT model

Parameters	Runner	Guide vanes	Return channels
D	400 mm	410 mm	516 mm
B	40 mm	40 mm	40 mm
n	7	22	11
α	26.5°	23.44°	30°

The hexahedral mesh is generated for this RPT model by decomposing the structured blocks. The computational mesh composed of six domains created on the return channels, the guide vane, the runner, the draft tube and the leakage system (Fig. 3). A mesh sensitivity study is carried out at the best efficiency point (BEP) to guarantee that the numerical simulation can capture the pressure pulsations as well, with different mesh densities used, as shown in Fig. 3(a).

Even if the sensitivity analysis highlights a mesh independent solution with about 2×10^5 elements for each runner passage (Fig. 3(a) A), the intensity and the extent of the local pressure pulsations appear to be correctly evaluated only with the number of mesh elements exceeding 3×10^5 for each passage (Fig. 3(a) B). To assure that the numerical solution can well capture the local pressure pulsations in the whole domain, the adopted number of elements is further increased to around 5.65×10^5 elements for each passage (Fig. 3(a) C). O-grids are adopted for the vanes in the guide vane with about 3.55×10^5 cells; for the runner with a total cells of about 3.7×10^5 and a y^+ values below 30 and for the return channel with

about 5.11×10^5 cells. A structured mesh with about 3.25×10^5 elements is built on the draft tube, with a y^+ value less than 30. In view of the influence of the leakage flow rate in the fluid under partial loads, the labyrinth seal is also modelled by several H-blocks, as shown in Figs. 3(a), 3(b).

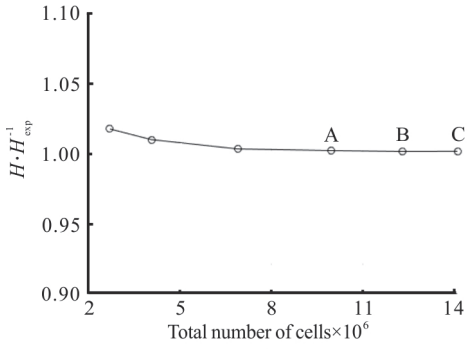

(a)

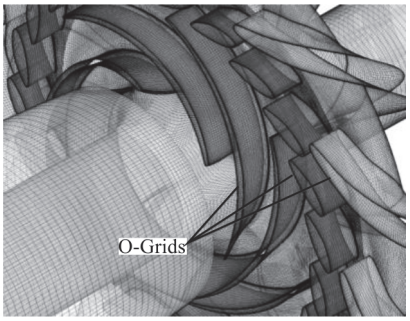

(b)

Fig. 3 Analysis of mesh sensitivity

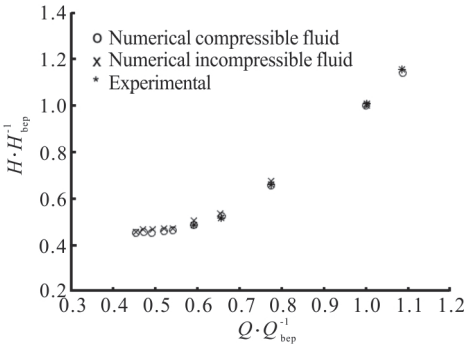

Fig. 4 Comparison between numerical and experimental head curves

2.1 *Validation of RPT model under stable operating conditions*

To validate this RPT model, the results in terms of the head under the steady operation condition at a constant rotation rate (600 rpm) are compared with the experimental results according to the ISO standards. The global measurements of the flow, the head and the efficiency are made following the IEC recommendations: 0.1% precision for the efficiency near the best efficiency point and 0.3% for the overall domain and the calibration of the instruments is performed on site[5].

The numerical analyses are conducted for both the incompressible and compressible fluids. The results are averaged for 10 runner revolutions after more than 20 revolutions for the sake of achieving a quasi-steady simulation convergence at a constant rotation rate (600 rpm). The comparison in terms of the head is shown in Fig. 4, indicating that the average numerical and experimental results are in good agreement, with an error smaller than 0.2% near the best efficiency point (BEP) and smaller than about 3.3% for partial loads (Fig. 4). In terms of the errors of the numerical results with respect to the experimental results, the model with the compressible water is doing better. The errors are likely to be caused by the practical limitations of the numerical model, but all the errors are in a reasonable range under the BEP condition.

2.2 *Numerical model for resolution*

The detached eddy simulation (DES) model is used for the unsteady calculations in this work where the steady result is accepted in the initialization. In the simulation of the rejecting load, the movement of the guide vanes is based on a specified closure law with a time step equal to a rotation of 1° (Fig. 6(a)). In all numerical simulations in this work, all the interfaces between the stator and rotor blocks are the standard transient sliding interfaces. The total pressure measured in the experiment is regarded as the inlet boundary condition. Due to the highly disturbed flow field at the outlet, an open condition with an average static pressure (equal to the measured value in the experiment) is used to fix the outlet boundary condition.

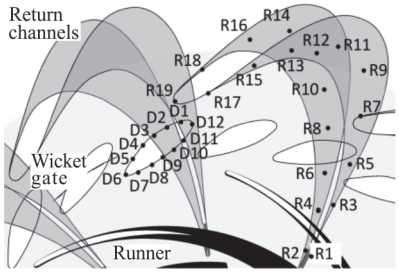

Fig. 5(a) Monitoring points on vanes

Furthermore, the obtained maximum Courant number is less than 3 for all studied flow rates, guaranteeing an accurate resolution of the transient details. The resultant root mean square (rms) values for the residuals are u momentum$\times10^{-5}$, v momentum$\times10^{-5}$, w momentum$\times10^{-6}$, and the turbulence kinetic energy$\times10^{-5}$.

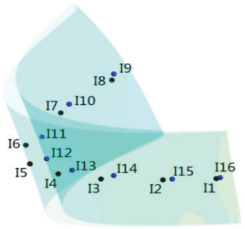

Fig. 5(b) (Color online) Monitoring points on blade

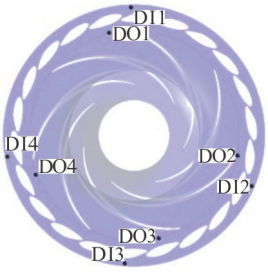

Fig. 5(c) (Color online) Monitoring points at the inlet and the outlet of guide vane

The transient flow characteristics of this model can be obtained by analyzing the signals of the mass flow, torque and pressure fluctuations in the frequency and time-frequency domains, Fig. 5 presents a scheme of the positions of the monitoring points for acquiring the related signals.

2.3 *Realization of continuous movement of guide vane*

To simulate the fast load reduction phase, a sudden closure of the guide vanes with the One Section Closure Law is considered in this case study[21-22]. The closure law of the guide vanes consists of three periods, an initial acceleration, a constant velocity closure and a negative acceleration before the end position (Fig. 6(a)). The guide vanes start to rotate from the position $\alpha = 23.44°$ (BEP), to the final position $\alpha = 5.79°$ as shown in Fig. 6(b).

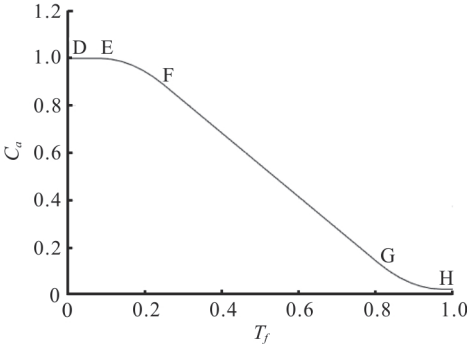

Fig. 6(a) Representations of guide vane closure law

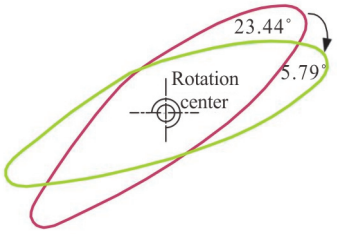

Fig. 6(b) (Color online) Vane positions at BEP and the minimum angle

The motion of all mesh nodes is controlled by the mesh motion function, currently limited to thedisplacement diffusion. By using the mesh motion model, the displacement on the domain boundary or in the sub-domain spreads to other mesh points determined by solving the equation $\nabla \times (\Gamma_{\text{disp}} \nabla \delta) = 0$. In this equation, δ is the displacement relative to the previous mesh node position, Γ_{disp} is the mesh stiffness which determines the degree of the node area moving together. This equation is particularly useful for determining the initial value in each iteration based on the time step, no matter in a steady or transient simulation. It is worth mentioning that the displacement diffusion model of the mesh motion is designed to preserve the relative mesh distribution of the initial mesh. In particular, if the initial mesh is relatively fine in some areas of the domain (for example, in the boundary layer), it will remain so after the solution (for stable domains or moving domains in a small region)[23].

In order to both increase the volume and preserve the quality of the prismatic elements close to the border, the "specified displacement" is adopted as the mesh motion method with a set mesh stiffness to allow for absorbing the main deformation far from the body for the domain movement in a small range. Instead, all guide vanes are moved to specified locations based on the closure law (Fig. 6). Upper and lower surfaces of the guide vane domain are set by using the "Unspecified Mesh Motion" method with the inlet and the outlet under the "Stationary" condition.

If one guide vane rotating center is (a,b,c), with the point (x,y,c) to represent the subdomain of the vane, with the runner rotating center point (x_c,y_c,c), where c is equal to the distance between the middle height of the guide vane and the center of the model (this center of the model is a variable, with the same z value as that of the points on the vane.), i represents the guide vane number (in this case $1 \le i \le 22$), r is the distance between the position of the point and the center of the model, the velocity of

the mesh motion depends on the guide vane closure law. The expression of the guide vane movement can be expressed as (Eqs. (1)-(6)):

$$\text{alpha}(i) = (a\tan 2(y - y_c), (x - x_c)) \quad (1)$$

$$\text{deltaalpha} = \text{velocity} \times \text{timestep} \quad (2)$$

$$\text{alpha}_{\text{new}}(i) = \text{alpha}(i) - \text{deltaalpha} \quad (3)$$

$$r = \sqrt{(x - x_c)^2 + (y - y_c)^2} \quad (4)$$

$$x_{\text{new}}(i) = r\cos[\text{alpha}_{\text{new}}(i)] + x_c \quad (5)$$

$$y_{\text{new}}(i) = r\cos[\text{alpha}_{\text{new}}(i)] + y_c \quad (6)$$

In the initial stage of the coupling iteration, because of the minimum surface angle, the system variables are not converged, both the flow field and the structure have not reached the final coupling state. Therefore, the flow load is prone to have a drastic change in a short moment, resulting in a large temporary local deformation of the structure, also resulting in a negative volume of the mesh and the collapse of the calculation, which seriously affects the reliability of the coupling system. Using the mesh stiffness coefficient can solve this kind of problems in theory, but the effect is very limited. Especially for a large scale mesh movement, the method illustrated in the last section is hard to ensure a high mesh quality.

In the present paper, the minimum surface angle is regarded as a standard of the mesh quality, to guarantee a quality mesh better than 60% during the dynamic closure of the guide vanes, and a wall sliding mesh technique is proposed. The numerical simulation of the guide vane continuous closure is realized by using this new dynamic mesh technique. The main idea of this wall sliding mesh technique is to force the mesh nodes to move along the vane profile with a special function of the rotated angle.

Combining the expression of the vane movement mentioned before, supposing that the number of the mesh nodes on each vane profile is k, j is the number of the mesh nodes $(1 \le j \le k)$, f is a coefficient which affects the velocity of the node movement; with the coefficients $f1$, $f2$ (relating to y values of points) and $f3$ (relating to the radius at each point) by using the software Autosignal software, $f4$ is the angle correction factor, the new expression for one vane with consideration of the wall sliding mesh can be expressed as (Eqs. (7)-(19)):

$$\text{alpha}(j)_{\text{initial}} = a\tan 2(y(j) - y_c), (x(j) - x_c) \quad (7)$$

$$\text{alpha}(j) = \text{if } (\text{alpha}(j)_{\text{initial}} < \pi, \text{alpha}(j)_{\text{initial}}$$

$$\text{if } (0 < \text{alpha}(j)_{\text{initial}}, \text{alpha}(j)_{\text{initial}} - 2\pi,$$

$$\text{alpha}(j)_{\text{initial}} + 2\pi)) \quad (8)$$

$$r = \sqrt{(x - x_c)^2 + (y - y_c)^2} \quad (9)$$

$$\text{alpha}_{\text{linearization}}(j) = \text{alpha}(j) \ (j = 1) \quad (10)$$

$$\text{alpha}_{\text{linearization}}(j) = \text{alpha}_{\text{linearization}}(j-1) + [\text{alpha}(k) -$$

$$\text{alpha}(1)] \ (2 \le j \le k) \quad (11)$$

$$r_{\text{linearization}}(j) = \text{alpha}(j), \ (j = 1) \quad (12)$$

$$r_{\text{linearization}}(j) = r(j-1) - \frac{r(j-1) - r(j)}{\text{alpha}(j-1) - \text{alpha}(j)} \cdot$$

$$[\text{alpha}(j-1) - \text{alpha}_{\text{linearization}}(j)] \ (2 \le j \le k) \quad (13)$$

$$x_{\text{linearization}}(j) = r_{\text{linearization}}(j)\cos[\text{alpha}_{\text{linearization}}(j)] \quad (14)$$

$$y_{\text{linearization}}(j) = r_{\text{linearization}}(j)\sin[\text{alpha}_{\text{linearization}}(j)] \quad (15)$$

$$\text{alpha}_{\text{new}}(j) = \text{alpha}(j) - \text{velocity} \times f \times \frac{\pi}{180} + f4 \quad (16)$$

$$r_{\text{new}}(j) = \left\{\sum_{j=1}^{k} f1(j)\sin[f2(j) \times 2\pi]\right\} \times \text{alpha}(j) +$$

$$\sum_{j=1}^{k} f3(j) \quad (17)$$

$$x_{\text{new}}(j) = r_{\text{new}}(j)\sin[\text{alpha}_{\text{new}}(j)] + x_c - x(j) \quad (18)$$

$$y_{\text{new}}(j) = r_{\text{new}}(j)\cos[\text{alpha}_{\text{new}}(j)] + y_c - y(j) \quad (19)$$

In the above expressions (Eqs. (7)-(19)), x_{new} and y_{new} represent the values set in the mesh motion, instead of the real coordinates of the points based on the model center, $z = 0$ is used for all vane settings of the displacement. $\text{alpha}_{\text{new}}(j)$ depends on $\text{alpha}(j)_{\text{initial}}$ which also relates to the closing law of the guide vane (shown in the equations as the velocity), with the velocity being a value relying on the openings of the vane with the unit of degree.

As for other vanes, the only thing needs to do is

to let the angle $= i \times 360° / k$, and all controlling functions are similar. This solution partially compensates the mesh distortion and the angle reduction with acceptable values in the rotation of the guide vanes. The mesh angle of the guide vane distribution is shown in Fig. 7 at some special positions.

3. Results and discussions

Figure 7 illustrates the distribution of the mesh angle at the special points D, E, F and G (Fig. 6). In this period of the load regulation scenario, the minimum face angle of the mesh is greater than 30°, and the mesh maintains the orthogonality basically. The results demonstrate that the wall sliding mesh technique is a good method to solve the problem of bad mesh quality, in a continuous simulation of the guide vane movement.

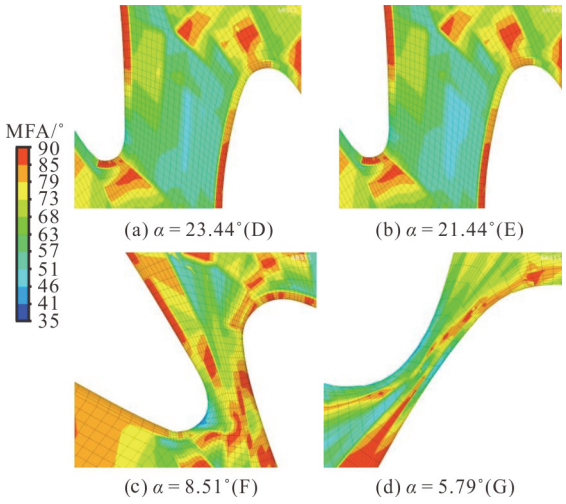

Fig. 7 (Color online) Distribution of mesh angle in guide vane domain at special points: D, E, F, G (Fig. 6)

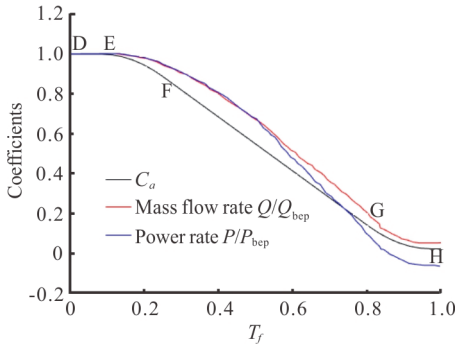

Fig. 8(a) (Color online) Mass flow and power rates of the RPT

Figure 8 shows the mass flow and the power rates of this RPT during the guide vane closure. The mass flow is decreased with a small delay when the guide vanes start to move at a fixed velocity. The flow rate is reduced quickly after the guide vanes are closed by about 40% of the rotation. Consistently, the power rate decrease is evident in the last phase of the closure procedure (Fig. 8(a)). In order to show the oscillations clearly, Fig. 8(a) is enlarged from $T_f = 0.4$ to $T_f = 0.45$ (Fig. 8(b)), to illustrate the mass flow pulsations in all vane channels during the transition between the operating points in detail, from $T_f = 0.4$ to $T_f = 0.45$: small pressure variations can be clearly observed and the maximum fluctuation range is about 0.5 kg/s.

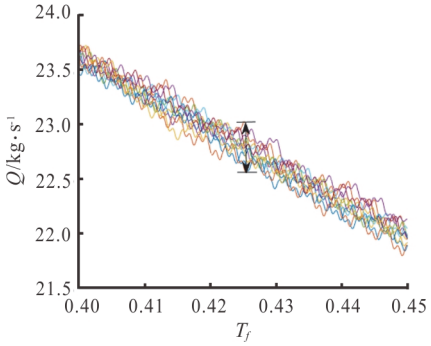

Fig. 8(b) (Color online) a detailed representation of Fig. 8(a) from $T_f = 0.4$ to $T_f = 0.45$

Figure 9 shows the streamlines in the domains including the return channels, the guide vane and the runner. At the beginning of the load rejection, the flow is regular and no vortex can be found. However, it is perturbed by a sort of unsteady stall phenomena in the runner channels characterized by the vortexes partially blocking the channels finally (Fig. 9(d)).

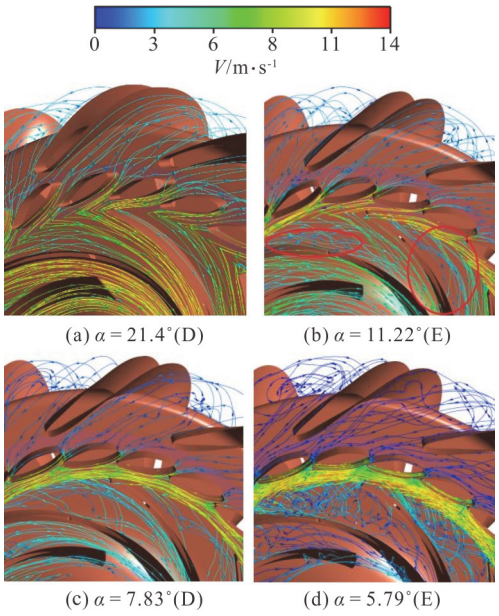

Fig. 9 (Color online) Streamlines in passages at special points

Starting from $T_f = 0.58$ (Fig. 9(a)), the streamline disorders begin to appear on the pressure side of the blades close to the runner inlet, and then the unstable flow looms large gradually in the runner passages and the intense flow separation is observed, especially in the period from G to H (Fig. 8(a)), where the flow vortexes are shown very clearly (Fig. 9(d)), all the runner blade passages are filled with large scale vortexes finally.

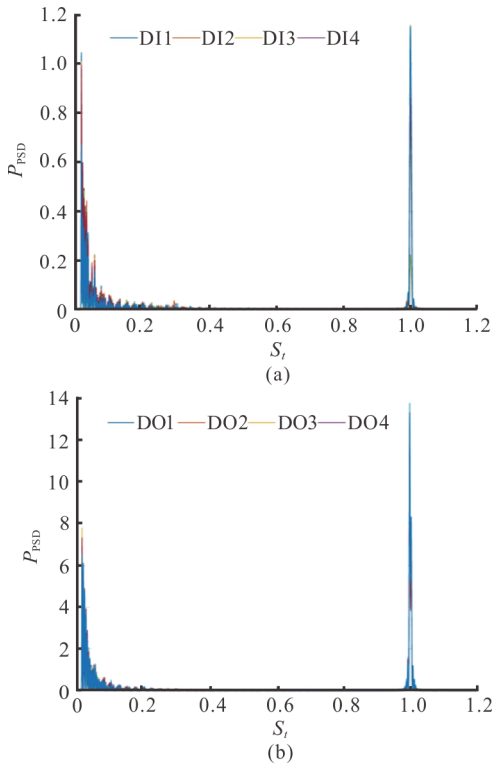

Fig.10 (Color online) Normalized power-spectra of pressure at guide vane inlet and outlet acquired from monitoring points of Fig. 5

At the beginning of the transient process, small vortex core regions can be observed in the runner passage, near the runner inlet. These vortex core regions are generated by the wakes of the guide vanes, and the flow separation vortices on the suction surfaces, mainly due to the interactions between the guide vanes and the runner blades (Fig. 9). The flow in the first two-thirds of the runner channels is disturbed by the onset of the flow detachments, whereas the remaining part of the blades is working properly (Fig. 9(c)). Note that at the inlet of the runner, the influence of the water ring is obviously responsible for the disorderly flow with grievous vortexes. However, at the end of the blade passage regions, the flow pattern is less chaotic than the front part with a bit normal and regular behavior before G (Fig. 9). Meanwhile, the decreasing flow is the main factor for the development and the enlargement of the regions of the flow separation, and for the onset of a back flow near the inlet throats (Figs. 9(a), 9(c)), and the further reductions of the flow lead to a full blockage of the runner passages (Fig. 9(d)).

The fluid in the return channels is relatively stable as compared with the fluid in other domains due to the fact that the flow passes the return channel before other parts, consequently, the flow pattern is not changed too much. In addition, a small number of vortexes appear when the guide vanes approach the terminus position (Fig. 9(d)), and the closure of the vanes leads to a significant flow rate drop, which also affects the fluid in the return channel.

The locations of the monitoring points (Fig. 5) are very important, because the rotor-stator interaction varies significantly along the passage. The maximum values of the blade passing frequency (BPF) can be observed near the guide vane trailing edge (Fig. 10). In addition, the value of the BPF at the outlet region of the guide vane is more than 10 times of that in the regions near the guide vane inlet.

In the guide vane, the flow rate shows a limited oscillation (Fig. 8(b)) with a frequency equal to the blade passage frequency after the guide vanes are closed by about 70% (Fig. 11). In the range of 70% and 85% of the vane closure, the higher frequencies disappear and some sub-tonal frequencies appear because of the effect of the instability in the return channels. Moreover, the blade passage frequency can be clearly measured from the flow rate oscillations in the guide vane at a higher angle closure (Fig. 11).

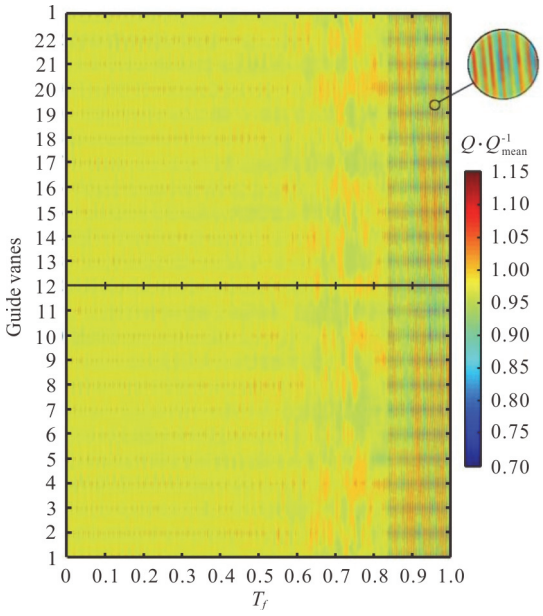

Fig.11 (Color online) Overview of flow rate evolution in all guide vane channels

From the combined action of the pressure and the flow rate variations over time, the non-constant torque of the guide vanes can be predicted. Figure 12 presents the auto spectra of the torque signals acquired on the guide vanes.

Depending on the flow field evolution during the guide vane closure, the auto spectra of the vanes torque signals (Fig. 12) are dominated by a peak $(St = 1)$, as expected, and the BPF is also observed in the spectrum due to the reflection from the stator parts $(St = 1)$, which is perturbed by the development of the unsteady phenomena as well.

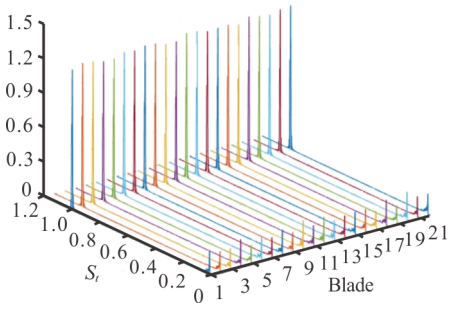

Fig. 12 (Color online) Torque factor versus St of diffuser vanes

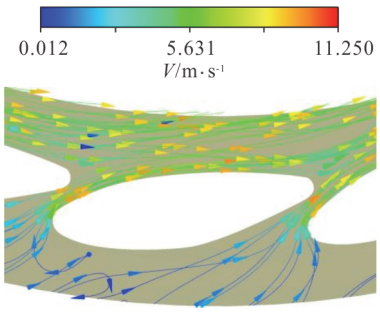

Fig. 13 (Color online) Water ring between guide vane outlet and runner inlet

The flow field in the guide vane during this transient period, owing to the throat spacing of the vanes keeps decreasing, which makes the flow velocity at the vane outlet rise rapidly in this region (Fig. 13). A closed water ring is formed in the gap space between the guide vane outlet and the runner blade inlet because of the vane closure, also with a rotating velocity along the circumferential direction similar to the case along the runner rotating direction (Fig. 13). It is worth mentioning that the water ring is gradually formed and becomes stronger with the time of the retirement, and this is also an important fact responsible for the unstable fluid in the runner passage.

Meanwhile, even when the flow rate approaches nearly to 0 at $T_f = 0.97$, the water ring still exists because the runner passages are blocked by the vortexes.

The dynamic fluid in the draft tube can be identified continuously by means of this new sliding mesh technique. Initially, the fluid in the draft tube is stable before the stage E, the flow in the runner passage is under a similar condition as at the BEP point because the mass flow is only dropped by about 5.88% before the stage F.

With the flow rate decreasing (F-G), the flow in the draft tube is affected significantly by the fluid near the runner outlet, moreover, the flow passes through the draft tube with a rotating speed, and a rotating direction similar to the runner rotating direction (Fig. 14).

According to the load variation (Fig. 6), the second stage sees a linear change which makes the mass flow fall to 7.23% directly, the fluid becomes unstable in the passage after $T_f = 0.58$ (with the mass flow lost about 37.35%) when the flow inside the draft tube is affected significantly by the flow from the runner outlet as compared with the fluid before this moment. The flow in the draft tube progressively gets greater with the distance from the hub, at $T_f = 0.64$, the flow in the draft tube disengages from the hub (Fig. 9(b)), at $T_f = 0.67$, the back

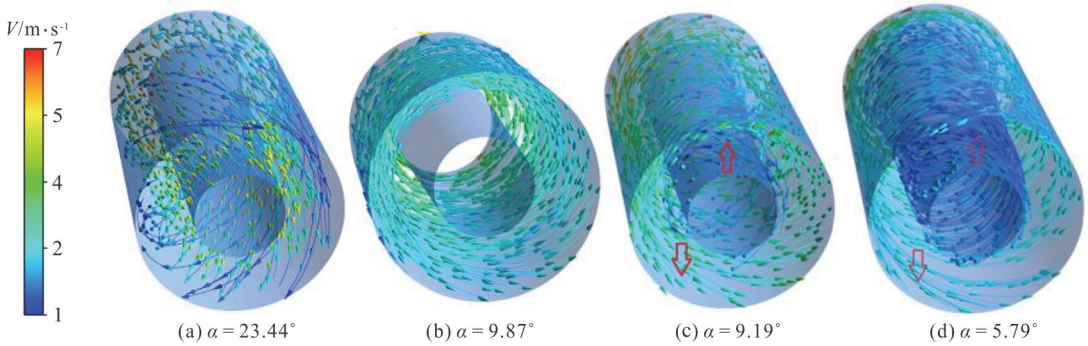

Fig.14 (Color online) Streamlines in the draft tube

flow appears while in the flow the reflux is formed and rotates around the hub in the opposite direction (Fig. 9(c)).

Gradually the flow in the draft tube is divided in two parts: one part of the fluid is around the hub to form the reflux, while the other part flows out along the wall of the draft tube (Fig. 14(d)). Moreover, the rotating directions of these two parts are opposite because the first part of the flow around the hub to form the reflux is affected by the vortexes, whilst the second part flow mainly comes from the runner outlet.

4. Conclusions

The dynamic simulations and the numerical analyses are carried out for a reversible turbine operating from the BEP point to the guide vane closure point in the turbine mode, the continuous guide vane movement can be realized through the adoption of the dynamic mesh based on the functions. The pressure, the flow rate and the torque acquired from the monitoring points over time are used to analyze the fluid during the rapid closure of the guide vanes. The major conclusions are as follows:

(1) This case study shows that a continuous assessment of the transient flow characteristics during the guide vane closure can be made by using the new method of the dynamic mesh.

(2) The fluid keeps stable at the beginning of the decreasing flow phase, whereas the vortexes appear from $T_f = 0.58$ (with the guide vane closed by about 67%), a small number of vortexes appear in the flow passage, which can be observed in the runner channels clearly, and the vortexes are progressively developed and block the whole flow passage, even a separated flow pattern is formed (with the guide vane closed by about 95%), which can be observed clearly.

(3) The mass flow decreases with a little delay when the guide vanes start to move at a fixed velocity rate. The flow rate is reduced quickly after the guide vanes are closed by about 40% of the rotation. Furthermore, with the reduction of the mass flow and the decrease of the distance between the guide vane outlet and the runner inlet, the closed water ring in this gap space is formed and rotates in the similar direction as the rotating runner, which is mainly responsible for the unstable fluid in the runner passage.

(4) The flow field in the draft tube is affected significantly after the guide vanes is closed by approximately 66%, and quickly the flow gathers to the wall and disengages from the hub when the vane is closed by about 73%. Then the reflux appears and rotates around the draft tube hub in the opposite direction as compared with the flow on the draft tube wall, and with these two flows two separated rotating water columns are finally formed. The two separated water columns are significantly important in causing the unit vibration.

However, this new method of the dynamic mesh also has a disadvantage, it can not guarantee a high quality mesh in narrow regions (in this case, we only used this new mesh method to the 95% guide vane closure), hence further studies will focus on finding another way to solve this problem. Furthermore, future studies could also include the analysis of the fluid induced noise, an aspect closely related to the safety issues and the lifespan of the unit. This will be implemented in the next research stage by following a similar approach which has been shown to be successful in the previously published paper [2].

Acknowledgement

This work was supported by the Research Start-Up Foundation of Northwest A&F University (Grant No. Z109021813).

References

[1] Deane J. P., Ó Gallachóir B. P., Mckeogh E. J. Techno-economic review of existing and new pumped hydro energy storage plant [J]. *Renewable and Sustainable Energy Reviews*, 2010, 14(4): 1293-1302.

[2] Sundararagavan S., Baker E. Evaluating energy storage technologies for wind power integration [J]. *Solar Energy*, 2012, 86(9): 2707-2717.

[3] Olimstad G. Characteristics of reversible-pump turbines [D]. Doctoral Thesis, Trondheim, Norway: Norwegian University of Science and Technology, 2012.

[4] Ren Y., Zheng Y., Li Y. Modeling and simulation of hybrid windpvpumped-storage system [J]. *Journal of drainage and irrigation machinery engineering*, 2011, 29(6): 518-522 (in Chinese).

[5] Zhang Y. N., Liu K. H., Li J. W. et al. Analysis of the vortices in the inner flow of reversible pump turbine with the new omega vortex identification method [J]. *Journal of Hydrodynamics,* 2018, 30(3): 463-469.

[6] Fu X., Li D., Wang H. et al. Influence of the clearance flow on the load rejection process in a pump-turbine [J]. *Renewable Energy,* 2018, 127: 310-321.

[7] Mao X. L., Zheng Y., Qu B. Hydraulic design of small mixed-flow reversible pump turbine [J]. *South to North Water Transfer and Water Science Technology,* 2014, 12(6): 123-126(in Chinese).

[8] Nilsson O., Sjelvgren D. Hydro unit start-up costs and their impact on the short term scheduling strategies of swedish power producers [J]. *IEEE Transactions on Power Systems*, 1997, 12(1): 38-44.

[9] Li D., Zuo Z., Wang H. et al. Review of positive slopes on pump performance characteristics of pump-turbines [J]. *Renewable and Sustainable Energy Reviews*, 2019, 112: 901-916.

[10] Nicolle J., Giroux A. M., Morissette J. F. CFD configurations for hydraulic turbine startup [J]. *IOP Conference Series: Earth and Environmental Science*, 2014, 22(3): 032021.

[11] Xiao J., Zhu E., Wang G. Numerical simulation of

emergency shutdown process of ring gate in hydraulic turbine runaway [J]. *Journal of Fluid Engineering*, 2012, 134(12): 124501.

[12] Trivedi C., Gandhi B. K., Cervantes M. J. et al. Experimental investigations of a model Francis turbine during shutdown at synchronous speed [J]. *Renewable Energy,* 2015, 83: 828-836.

[13] Côté P., Dumas G., Moisan É. et al. Numerical investigation of the flow behavior into a Francis runner during load rejection [J]. *IOP Conference Series: Earth and Environmental Science*, 2014, 22(3): 032023.

[14] Trivedi C., Gandhi B., Miche C. J. l. Effect of transients on francis turbine runner life: A review [J]. *Journal of Hydraulic Research,* 2013, 51(2): 121-132.

[15] Liu X. L., Zheng Y., Gao Y. N. Closing law of guide vane of reversible pump-turbine for pumped storage power stations [J]. *Water Resources and Power*, 2011, 29(6): 151-153(in Chinese).

[16] Derakhshan S., Nourbakhsh A. Experimental study of characteristic curves of centrifugal pumps working as turbines in different specific speeds [J]. *Experimental Thermal and Fluid Science*, 2008, 32(3): 800-807.

[17] Yang S. S., Derakhshan S., Kong F. Y. Theoretical, numerical and experimental prediction of pump as turbine performance [J]. *Renewable Energy*, 2012, 48(6): 507-513.

[18] Yang J., Pavesi G., Yuan S. et al. experimental characterization of a pump turbine in pump mode at hump instability region [J]. *Journal of Fluid Engineering,* 2015, 137(5): 051109.

[19] Mao X., Giorgio P., Zheng Y. Francis-type reversible turbine field investigation during fast closure of wicket gates [J]. *Journal of Fluid Engineering*, 2018, 140(6): 061103.

[20] Li X., Chang J., Chen P. Wicket gate closure control law to improve the transient of a water turbine [J]. *Advanced Materials Research*, 2013, 732(733): 451-456.

[21] Cui H., Fan H., Chen N. Optimization of wicket-gate closing law considering different cases [J]. *IOP Conference Series: Earth and Environmental Science*, 2012, 15(5): 052008.

[22] Tang T. Moving mesh methods for computational fluid dynamics [J]. *Contemporary Mathematics*, 2005, 383(8): 141-173.

[23] Zheng Y., Chen Y. J., Mao X. L. et al. Pressure pulsation characteristics and its impact on flow-induced noise in mixed-flow pump [J]. *Transactions of the Chinese Society of Agricultural Engineering*, 2015, 31(23): 67-73(in Chinese).